

IMECE2012-85675

## HYPERELASTIC AND VISCOELASTIC PROPERTIES OF BRAIN TISSUE IN TENSION

### BADAR RASHID

School of Mechanical and Materials Engineering,  
University College Dublin, Belfield  
Dublin 4, Ireland  
seebadar@yahoo.com,  
Badar.Rashid@ucdconnect.ie

### MICHEL DESTRADE

School of Mathematics, Statistics and Applied  
Mathematics, National University of Ireland  
Galway, Galway, Ireland  
michel.destrade@nuigalway.ie

### MICHAEL D GILCHRIST

School of Mechanical and Materials Engineering,  
University College Dublin, Belfield  
Dublin 4, Ireland  
michael.gilchrist@ucd.ie

### ABSTRACT

Mechanical characterization of brain tissue at high loading velocities is particularly important for modelling Traumatic Brain Injury (TBI). During severe impact conditions, brain tissue experiences a mixture of compression, tension and shear. Diffuse axonal injury (DAI) occurs in animals and humans when the strains and strain rates exceed 10% and 10/s, respectively. Knowing the mechanical properties of brain tissue at these strains and strain rates is thus of particular importance, as they can be used in finite element simulations to predict the occurrence of brain injuries under different impact conditions.

In this research, uniaxial tensile tests at strain rates of 30, 60 and 90/s up to 30% strain and stress relaxation tests in tension at various strain magnitudes (10% - 60%) with an average rise time of 24 ms were performed. The brain tissue showed a stiffer response with increasing strain rates, showing that hyperelastic models are not adequate and that viscoelastic models are required. Specifically, the tensile engineering stress at 30% strain was  $3.1 \pm 0.49$  kPa,  $4.3 \pm 0.86$  kPa,  $6.5 \pm 0.76$  kPa (mean  $\pm$  SD) at strain rates of 30, 60 and 90/s, respectively. The Prony parameters were estimated from the relaxation data. Numerical simulations were performed using a one-term Ogden model to analyze hyperelastic and viscoelastic behavior of brain tissue up to 30% strain. The material parameters obtained in this study will help to develop biofidelic human brain finite

element models, which subsequently can be used to predict brain injuries under impact conditions.

### INTRODUCTION

Traumatic brain injury (TBI) occurs when a sudden trauma causes damage to the brain. Most TBIs are due to transportation accidents involving automobiles, motorcycles, bicycles, pedestrians and are also due to sports events. *Concussion* is the most minor and the most common type of TBI, whereas *diffuse axonal injury* (DAI) is the most severe form of injury which involves damage to individual nerve cells (*neurons*) and loss of connections among neurons. To gain a better understanding of the mechanisms of TBI, several research groups have developed numerical models which contain detailed geometric descriptions of the anatomical features of the human head, in order to investigate internal dynamic responses to multiple loading conditions [1-6]. However, the biofidelity of these models is highly dependent on the accuracy of the material properties used to model biological tissues; therefore, more systematic research on the constitutive behavior of brain tissue under impact is essential.

On a microscopic scale, the brain is made up of billions of cells that interconnect and communicate [7]. One of the most pervasive types of injury following even a minor trauma is damage to the nerve cell's axon through shearing during DAI. DAI in animals and human has been hypothesized to occur at macroscopic shear strains of 10% - 50% and strain rates of

approximately 10 – 50/s [8, 9]. Several studies have been conducted to determine the range of strain and strain rates associated with DAI. Studies conducted by Morrison et al., [10-12] suggested that the brain cells are significantly damaged at strains > 0.10 and strain rates > 10/s.

Over the past three decades, several research groups have investigated the mechanical properties of brain tissue in order to establish constitutive relationships over a wide range of loading conditions. Mostly dynamic oscillatory shear tests were conducted [7, 13-22] and unconfined compression tests [20, 23-28]. However, only a limited number of tensile tests has been conducted [29-31] so far.

In this study, mechanical properties of porcine brain tissue have been determined by performing tension tests at 30, 60 and 90/s strain rates up to 30% strain. The loading rates in the present study approximately cover the range of strain rates as revealed during TBI investigations by various research groups [8-12, 32-34]. To the authors' knowledge, no experimental data for brain tissue in tension at these dynamic strain rates is available except Tamura et al. [30], who performed tests at 0.9, 4.3 and 25/s; the fastest rate was closest to impact speeds.

## MATERIALS AND METHOD

### Specimen Preparation

Ten fresh porcine brains from approximately six month old pigs were collected approximately 6 h after death from a local slaughter house and tested within 4 h. Each brain was preserved in a physiological saline solution (0.9% NaCl /154 mmol/L) at 4 to 5°C during transportation. All samples were prepared and tested at a room temperature ~ 22 °C. Cylindrical specimens containing mixed white and gray matter were prepared as shown in Fig.1.

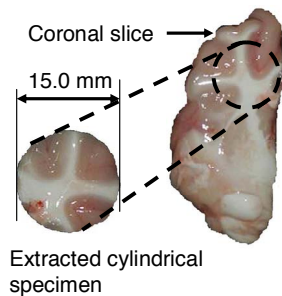


Fig. 1: Specimen extraction from the brain tissue

The actual diameter and height of specimens measured before testing were  $15.1 \pm 0.1$  mm and  $10.0 \pm 0.1$  mm (mean  $\pm$  SD) respectively. Miller and Chinzei [29] also used a sample height of 10.0 mm during tension tests at quasistatic velocities (0.005, 5.0 and 500 mm/min). The time elapsed between harvesting of the first and the last specimens from each brain was 16 ~ 20 minutes.

### Experimental Setup

A *High Rate Tension Device (HRTD)* was designed and calibrated to perform tensile tests at strain rates of 30, 60 and 90/s to characterize the behavior of brain tissue under TBI conditions [35]. The experimental setup was changed in order to perform tests with 10.0 mm specimen thickness, as shown in Fig. 2. The major components of the apparatus include a *servo motor actuator* (stroke length: 700 mm, maximum velocity: 1500 mm/s, *LEFB32T-700*, SMC Pneumatics), two *5 N load cells* (GSO series -5 to +5 N, Transducer Techniques), *Displacement Transducer* (ACT1000 LVDT, RDP Electronics) with a range  $\pm 25$  mm. The load cell was calibrated against known masses for the conversion of measured voltage to load (Newton). An integrated instrumentation amplifier (AD 623 G = 100, Analog Devices) with low-pass filter having a cut-off frequency of 10 kHz was used. The amplified signal was analyzed through a data acquisition system with a sampling frequency of 10 kHz. The force (N) and displacement (mm) data against time (s) were recorded for the tissue experiencing 30% strain.

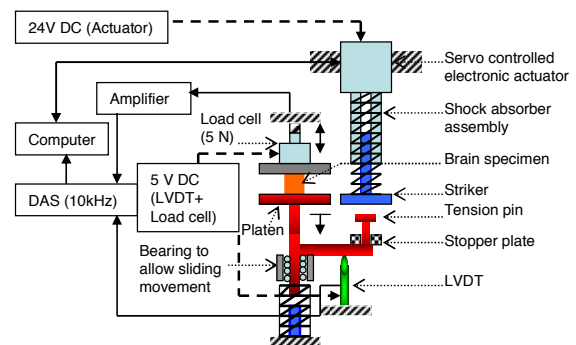


Fig. 2: Major components of high rate tension device (HRTD) and their interaction. Brain specimen is attached between the top and lower platens.

### Operation of HRTD

Before the actual tests, it was essential to attach the brain specimen with the platens by adopting a reliable method. We used surgical glue (Cyanoacrylate, Low-viscosity Z105880–1EA, Sigma-Aldrich) for the attachment of the specimens. The surfaces of the platens were first covered with a masking tape substrate to which a thin layer of surgical glue was applied. The top platen, which was attached to the 5 N load cell, was then lowered slowly so as to just touch the top surface of the specimen. One minute settling time was sufficient to ensure proper adhesion of the specimen to the platens. The *striker* attached to the electronic actuator (see Fig. 2) moved at a particular velocity to strike the *tension pin* which was rigidly attached to the lower platen as shown in Fig. 2. During the tests, the top platen remained stationary while the lower platen moved down to produce the required tension in the specimen.

## HYPERELASTIC CONSTITUTIVE MODELS

In general, an isotropic hyperelastic incompressible material is characterized by a strain-energy density function  $W$  which is a function of two principal strain invariants only:  $W = W(I_1, I_2)$ , where  $I_1$  and  $I_2$  are defined as [36],

$$I_1 = \lambda_1^2 + \lambda_2^2 + \lambda_3^2, \quad (1)$$

$$I_2 = \lambda_1^2 \lambda_2^2 + \lambda_1^2 \lambda_3^2 + \lambda_2^2 \lambda_3^2. \quad (2)$$

Here,  $\lambda_1^2, \lambda_2^2, \lambda_3^2$  are the squares of the principal stretch ratios, linked by the relationship  $\lambda_1 \lambda_2 \lambda_3 = 1$ , due to incompressibility. Due to symmetry and incompressibility, the stretch ratios are now of the form

$$\lambda_1 = \lambda, \quad \lambda_2 = \lambda_3 = \frac{1}{\sqrt{\lambda}} \quad (3)$$

where  $\lambda \geq 1$  is the stretch ratio in the direction of tension. Also, Eqs. (1) and (2) give

$$I_1 = \lambda^2 + 2\lambda^{-1}, \quad I_2 = \lambda^{-2} + 2\lambda, \quad (4)$$

so that  $W$  is now a function of  $\lambda$  only. The experimentally measured nominal stress was then compared to the predictions of the hyperelastic models from the relation [36],

$$S_{11} = \frac{d\tilde{W}}{d\lambda}, \quad \text{where } \tilde{W}(\lambda) \equiv W(\lambda^2 + 2\lambda^{-1}, \lambda^{-2} + 2\lambda), \quad (5)$$

The constitutive models were fitted to the stress-stretch data for strains up to 30%. The fitting was performed using the *lsqcurvefit.m* function in Matlab 6.9.

### Fung Strain Energy Function

The Fung isotropic strain energy [37, 38] depends on the first strain invariant only:

$$W = \frac{\mu}{2b} \left[ e^{b(I_1-3)} - 1 \right] \quad (6)$$

It yields the following nominal stress component  $S_{11}$  along the  $x_1$  - axis,

$$S_{11} = \mu e^{b(\lambda^2 + 2\lambda^{-1} - 3)} (\lambda - \lambda^{-2}) \quad (7)$$

Here  $\mu > 0$  (infinitesimal shear modulus) and  $b > 0$  (stiffening parameter) are the two constant material parameters to be adjusted in the curve-fitting exercise.

### Gent Strain Energy Function

The Gent isotropic strain energy [39] also depends on the first strain invariant only, as

$$W(I_1) = -\frac{\mu}{2} J_m \ln \left( 1 - \frac{I_1 - 3}{J_m} \right) \quad (8)$$

It yields the following nominal stress  $S_{11}$  along the  $x_1$  - axis

$$S_{11} = \frac{\mu J_m}{J_m - \lambda^2 - 2\lambda^{-1} + 3} (\lambda - \lambda^{-2}) \quad (9)$$

Here  $\mu > 0$  (infinitesimal shear modulus) and  $J_m > 0$  are two constant material parameters to be optimized in the fitting exercise.

### Ogden Strain Energy Function

Most of the mechanical test data available for brain tissue in the literature are fitted with an Ogden hyperelastic function. The one-term Ogden hyperelastic function is given by

$$W = \frac{2\mu}{\alpha^2} (\lambda_1^\alpha + \lambda_2^\alpha + \lambda_3^\alpha - 3) \quad (10)$$

It yields the following nominal stress  $S_{11}$ .

$$S_{11} = \frac{2\mu}{\alpha} \left\{ \lambda^{\alpha-1} - \lambda^{-\left(\frac{\alpha}{2}+1\right)} \right\} \quad (11)$$

Here  $\mu > 0$  is the infinitesimal shear modulus, and  $\alpha$  is a stiffening parameter.

## RESULTS

### Tensile Experiments

Ten tensile tests on cylindrical specimens were performed at each strain rate of 30, 60 and 90/s up to 30% strain (see Fig. 3) in order to analyze experimental repeatability and behavior of tissue at a particular loading velocity. The velocity of the platen producing extension in the brain tissue was adjusted to 300, 600 and 900 mm/s to attain approximate strain rates of 30, 60 and 90/s, respectively. Force (N) and displacement (mm) data measured directly at a sampling frequency of 10 kHz were converted to engineering stress (kPa) – time (s) for each strain rate.

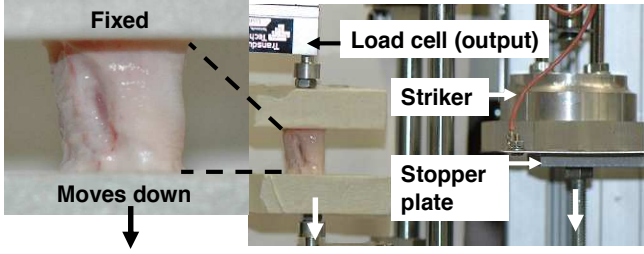


Fig. 3: Brain specimen fully stretched to achieve 30% strain at dynamic strain rates (30 – 90/s)

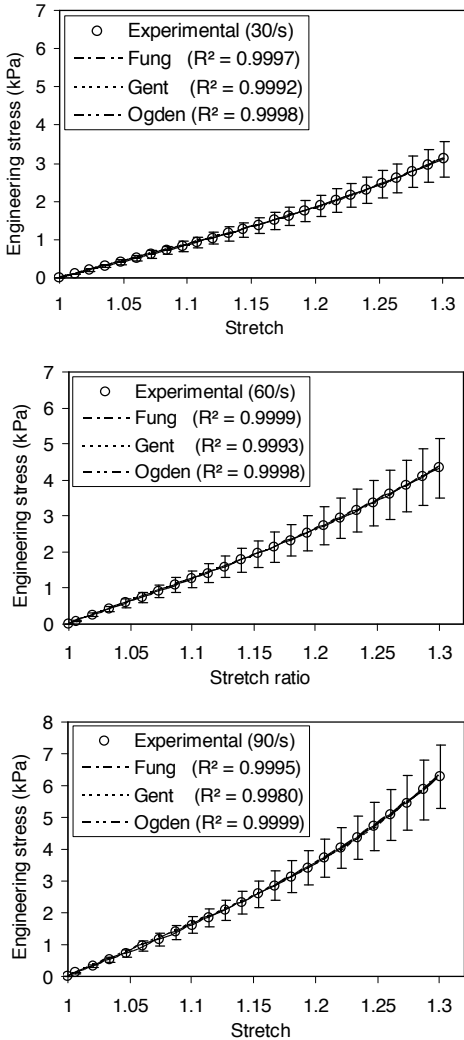


Fig. 4: Fitting of constitutive models to average experimental data

The average engineering stress – stretch curves at each loading rate were used for fitting to hyperelastic isotropic constitutive models (Fung, Gent and Ogden models) mentioned in Eqs. (7), (9) and (11). Excellent fit is achieved for all models (coefficient

of determination:  $0.9980 < R^2 \leq 0.9999$ ) as shown in Fig. 4. All best fit material parameters ( $\mu, \alpha, b, J_m$ ) derived after fitting strain energy functions to each experimental engineering stress – stretch profile are summarized in Table 1. Although the fit is excellent at each given strain rate, the hyperelastic models cannot capture the stiffening of the material with increasing strain rates. Therefore nonlinear viscoelastic modelling is required.

Table 1 – Material parameters derived after fitting of models to experimental data. All  $\mu$  are in Pa (mean) and  $\mu > 0$

1/s	Fung model		Gent model		Ogden model	
	$\mu$	$b$	$\mu$	$J_m$	$\mu$	$\alpha$
30	3047	1.68	3114	0.86	2780	6.0
	$R^2 = 0.9997$		$R^2 = 0.9991$		$R^2 = 0.9997$	
60	4458	1.5	4548	1.15	4112	5.63
	$R^2 = 0.9998$		$R^2 = 0.9993$		$R^2 = 0.9998$	
90	5739	2.19	5962	0.94	5160	6.95
	$R^2 = 0.9995$		$R^2 = 0.9979$		$R^2 = 0.9999$	

#### Young's Moduli of Brain Tissue

Here, the Young's moduli  $E_1, E_2$  and  $E_3$  are calculated from the tangent to the stress – strain curve corresponded to the strain ranges of 0 – 0.1, 0.1 – 0.2 and 0.2 – 0.3, respectively and are summarized in Table 2. Morrison et al., [11] assumed a Young's modulus,  $E$  of 10 kPa in their FE model to predict the strain field in a stretched culture of rat-brain tissue, in which the maximum strain and strain rates were 30% and 50/s respectively. This compares well with the mean Young's modulus,  $E_1$  (strain range: 0 – 0.1) estimated in this study, i.e.,  $11.68 \pm 3.79$  (kPa), as indicated in Table 2.

Table 2 – Young's moduli of brain tissue at each strain rate (mean  $\pm$  SD)

(1/s)	$E_1$ (kPa)	$E_2$ (kPa)	$E_3$ (kPa)
Range	0 – 0.1	0.1 – 0.2	0.2 – 0.3
30/s	$8.12 \pm 2.38$	$19.2 \pm 3.60$	$29.46 \pm 4.28$
60/s	$10.86 \pm 3.74$	$28.0 \pm 6.46$	$41.05 \pm 6.14$
90/s	$16.08 \pm 5.25$	$35.6 \pm 7.74$	$60.73 \pm 7.50$
<b>Mean</b>	<b><math>11.68 \pm 3.79</math></b>	<b><math>27.6 \pm 5.93</math></b>	<b><math>43.75 \pm 5.97</math></b>

We observe that the maximum engineering stress at 30% strain at strain rates of 30, 60 and 90/s was  $3.1 \pm 0.49$  kPa,  $4.3 \pm 0.86$  kPa,  $6.5 \pm 0.76$  kPa (mean  $\pm$  SD), respectively. The tissue stiffness clearly increases with the increase in loading velocity.

## VISCOELASTIC MODEL

Many nonlinear viscoelastic models have been formulated, but Fung's theory [40] of quasi-linear viscoelasticity (QLV) is probably the most widely used due to its relative simplicity. To account for the time-dependent mechanical properties of brain tissue, the stress-strain relationship is expressed as a single hereditary integral (similar approach has been adopted earlier [29, 41, 42]),

$$S(t) = \frac{2\mu}{\alpha} \int_0^t G(t-\tau) \frac{d}{d\tau} \left( \lambda^{\alpha-1} - \lambda^{\left(\frac{\alpha}{2}+1\right)} \right) d\tau \quad (12)$$

Here,  $S(t)$  is the nominal tensile stress component,  $\mu$  is the initial shear modulus in the undeformed state, and  $\alpha$  is a stiffening parameter derived from the one-term Ogden model (Eq. 10 and 11), where  $\mu > 0$ . The relaxation function  $G(t)$  is defined in terms of Prony series parameters:

$$G(t) = \left[ 1 - \sum_{k=1}^n g_k (1 - e^{-t/\tau_k}) \right] \quad (13)$$

where  $\tau_k$  are the characteristic relaxation times, and  $g_k$  are the relaxation coefficients. In order to estimate material parameters with physically meaningful interpretation, we propose to solve Eq. 12 in two simple steps.

### Force Relaxation in Tension

Force relaxation tests in tension were performed on cylindrical specimens ( $10.0 \pm 0.1$  mm thick and  $15.0 \pm 0.1$  mm diameter). Here, 64 specimens were extracted from 8 brains (4 samples from each cerebral hemisphere). Ten force relaxation tests were performed at each strain (10% - 60%) in order to investigate the response of brain tissue to a step-like strain.

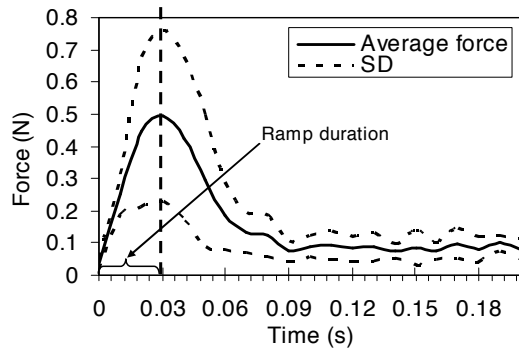


Fig. 5: Brain tissue force profiles obtained after ramp and hold relaxation tests. The average force and standard deviation (SD) is based on tests conducted at various strain magnitudes (10% - 60%)

The specimens were stretched at various loading levels (300 – 700 mm/s) and then held at the same position while measuring the relaxation force. The average rise time measured from the force relaxation experiments was approximately 24 milliseconds (ms) as shown in Fig. 5. The peak force relaxed by approximately 83% up to 0.1 s, and then it continuously decreased gradually up to 0.2 s. The dramatic decrease in force reveals the highly viscoelastic nature of brain tissue.

### Estimation of Viscoelastic Parameters

As a first step, curve fitting of the instantaneous response of a one-term Ogden model (Eq. 11) using experimental data at the maximum loading velocity (strain rate: 90/s) was performed to estimate  $\mu$  and  $\alpha$ . Thereafter, Eq. 12 was convenient to solve in Matlab 6.9 by using *gradient* and *conv* functions. The *gradient* function was used in order to determine the velocity

$$\text{vector} \frac{d}{d\tau} \left( \lambda^{\alpha-1} - \lambda^{\frac{\alpha}{2}-1} \right) \text{ from the experimentally measured}$$

displacement,  $\lambda$ , and time,  $\tau$ . Also, a *conv* function was used to convolve relaxation function (Eq. 12) with velocity vector. The coefficients of the relaxation function were optimized using *nlinfit* and *lsqcurvefit* to minimize error between the experimental stress data and Eq. (12). The derived Ogden parameters are  $\mu = 5160$  Pa and  $\alpha = 6.95$ . Similarly, we estimated Prony parameters ( $g_1 = 0.5837$ ,  $g_2 = 0.2387$ ,  $\tau_1 = 0.02571$  s,  $\tau_2 = 0.0257$  s) from a two-term relaxation function using Matlab functions discussed above. These material parameters can be used in ABAQUS software in order to analyze nonlinear viscoelastic behavior of brain tissue.

## FINITE ELEMENT SIMULATIONS

### Hyperelastic Simulations

Numerical simulations were performed by applying various boundary conditions using ABAQUS 6.9/ Explicit to mimic experimental conditions. A mass density of  $1040 \text{ kg/m}^3$  and 9710 hexagonal C3D8R elements were used for the brain part. The bottom surface of the cylindrical specimen was displaced in order to achieve 30% strain, whereas the top surface was constrained in all directions. Before numerical simulations, mesh convergence analysis was carried out by varying mesh density. The mesh was considered converged when there was a negligible change in the numerical solution (0.9%) with further mesh refinement. The total number of elements for the specimen was 2720 with average simulation time of 60 s. An excellent agreement between the experimentally measured forces (N) and the numerical forces (N) was obtained after the simulations, as shown in Fig. 6.

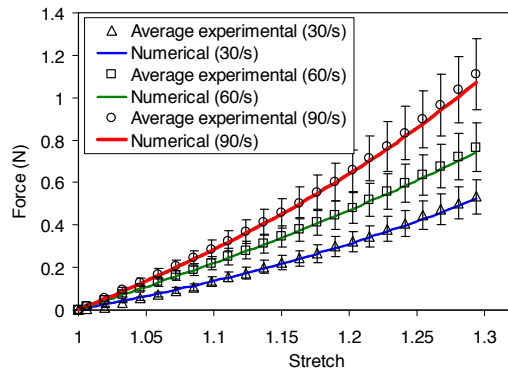


Fig. 6: Excellent agreement between the experimental and numerical results

The reaction forces contours are positive at the moving end and negative at the stationary end of the cylindrical specimen; however, the magnitudes of these forces remain the same at both ends of the specimen, as shown in Fig. 7.

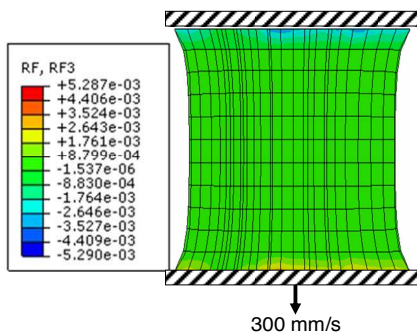


Fig. 7: Reaction force contours after the simulation

#### Nonlinear Viscoelastic Simulations

Numerical simulations were performed using both Ogden parameters ( $\mu = 5160$  Pa and  $\alpha = 6.95$ ) and viscoelastic parameters ( $g_1 = 0.5837$ ,  $g_2 = 0.2387$ ,  $\tau_1 = 0.02571$  s,  $\tau_2 = 0.0257$  s) in ABAQUS 6.9. Simulations were performed in order to analyze the reduction in force (N) profiles with the increase in relaxation time,  $t = 0.01, 0.05$  and  $0.15$  s (excluding rise time as shown in Fig. 5). Comparison of force profiles after the hyperelastic and nonlinear viscoelastic simulations are shown in Fig.8. There is approximately a 58% reduction from hyperelastic to nonlinear viscoelastic force (N) at  $t = 0.05$  s (at maximum stretch ratio of 1.3) as clearly depicted in Fig. 8. A similar reduction is also observed (approximately 40%) in nonlinear viscoelastic force from  $t = 0.05$  to  $0.15$  s, which shows the typical viscoelastic nature of brain tissue. Simulations were also performed to analyze engineering stress contour patterns by using the already derived hyperelastic and nonlinear viscoelastic parameters as shown in Fig. 9.

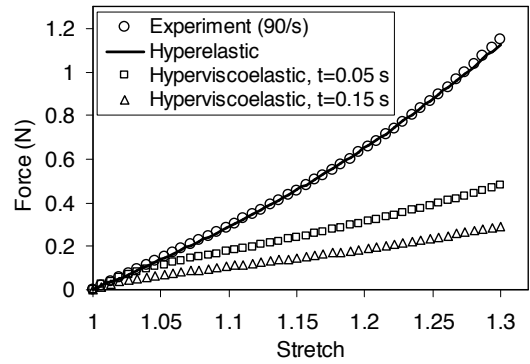


Fig. 8: Comparison of experimental and numerical force (N) profiles (hyperelastic and hyperviscoelastic force) after the simulations

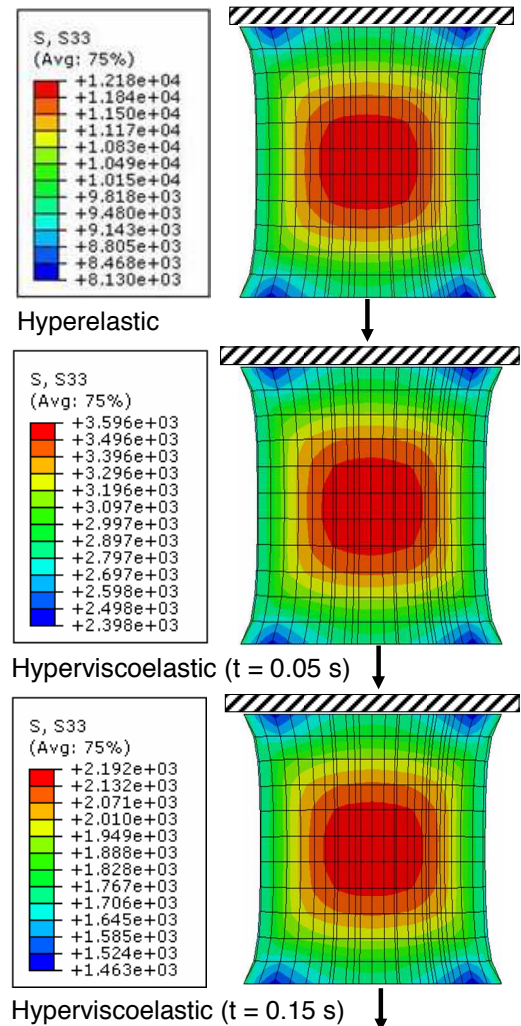


Fig. 9: There is no significant variation in engineering stress contours between hyperelastic and nonlinear viscoelastic simulations

It is clearly evident in Fig. 9 that only stress magnitudes are decreasing with the increase in relaxation time ( $t = 0.05$  to  $0.15$  s), while the stress contour patterns are approximately the same in all the cases. The maximum stress contours exist in the middle of the specimen, which symmetrically expands towards the edges of the cylindrical specimen. Inhomogeneous deformation of the specimen is expected with the decrease in specimen thickness / aspect ratio (diameter/height); however this important aspect of our experimental protocol has already been elaborated in a separate study [43].

## DISCUSSION

In this research, the properties of porcine brain tissue in extension have been determined up to 30% strain at strain rates of 30, 60 and 90/s by using a custom-designed HRTD. The characterization of brain tissue in tension at high strain rates is crucial in understanding the mechanism of TBI under impact conditions. Force relaxation experiments in tension at various strain magnitudes (10% - 60% strain) were performed with an approximate rise time of 24 ms. The nonlinear viscoelastic model adopted in this study can be implemented using Matlab 6.9 to estimate time-dependent Prony parameters. The parameters can be used for hyperviscoelastic simulations of brain tissue by using ABAQUS software.

Based on the one-way ANOVA test, there was no significant difference ( $p = 0.9254$ ) between the experimental and numerical force (hyperelastic) as shown in Fig. 8. An excellent agreement between the experimental and numerical results indicates that a one-term Ogden model is appropriate to characterize the behavior of the brain tissue up to 30% strain. The *accumulated artificial strain energy* (ALLAE), used to control *hourglass deformation* during numerical simulations, was also analyzed. It was observed that ALLAE for the whole model as a percentage of the total strain energy was 0.75%. The low percentage of artificial strain energy ( $\leq 0.85\%$ ) observed during the simulations indicates that hourglassing is not a problem.

Miller and Chinzei [29] performed tensile tests at room temperature ( $\sim 22^\circ\text{C}$ ) on cylindrical specimens of porcine brain tissue (diameter  $\sim 30$  mm; height  $\sim 10$  mm). The specimens were attached using surgical glue. Tamura et al. [30] also performed tensile tests at similar temperatures ( $25 - 28^\circ\text{C}$ ) on cylindrical specimens of porcine brain tissue (diameter  $\sim 14.2$  mm; height  $\sim 14.4$  mm), although they used a quench-freeze method to attach their specimens. The comparison of initial elastic moduli,  $E$  (Pa) at comparable strain rates is presented in Table 3. It is clearly observed that the elastic modulus at a strain rate of 0.9/s (Tamura et al. [30]) is approximately 8 times higher than that measured at 0.64/s strain rate (Miller and Chinzei [29]). Moreover, elastic modulus at a strain rate of 25/s (Tamura et al. [30]) is approximately 2.3 time higher than at 30/s strain rate (present study).

Table 3 – Comparison of initial elastic moduli,  $E$  at strain range (0 – 10%)

Reference	Strain rates: 1/s	$E$ (Pa)
Miller and Chinzei [29]	0.0064, 0.64	530 at 0.64/s
Tamura et al. [30]	0.9, 4.3, 25	4200 at 0.9/s 18600 at 25/s
Present study	30, 60, 90	8120 at 30/s

It is possible that the stiffer moduli measured by Tamura et al. [30] were a consequence of their brain specimens having been frozen for 1 h at  $-20^\circ\text{C}$  prior to coring out. Such freezing processes usually change the mechanical properties of brain tissue.

## CONCLUSIONS

The following results can be concluded from this study:

- (i) – One-term Fung, Gent and Ogden models provide excellent fitting to experimental data up to 30% strain.
- (ii) – Excellent agreement between the experimental and numerical engineering stresses indicates that the Ogden strain energy function is fully able to characterize the behavior of brain tissue in tension up to 30% strain. This model is readily available in ABAQUS/6.9 for numerical analysis.
- (iii) – Time dependent Prony parameters can be utilized with the Ogden hyperelastic parameters to perform nonlinear viscoelastic analysis of the brain tissue in ABAQUS/6.9.
- (iv) – The test apparatus (HRTD) can be used for soft biological tissues for the tension tests with confidence at strain rates  $\leq 90$ /s.

## ACKNOWLEDGMENT

The authors thank Dr. John D. Finan of Columbia University for his valuable input regarding implementation of the nonlinear viscoelastic model. This work was supported for the first author by a Postgraduate Research Scholarship awarded by the Irish Research Council for Science, Engineering and Technology (IRCSET), Ireland.

## NOMENCLATURE

$I_1, I_2$	= principal strain invariants
$W$	= strain-energy density function
$\lambda_1^2, \lambda_2^2, \lambda_3^2$	= principal stretch ratios
$\mu > 0$	= infinitesimal shear modulus (Pa) for Fung, Gent and Ogden models
$b > 0$	= Fung's stiffening parameter
$J_m > 0$	= Gent's stiffening parameter
$\alpha$	= Ogden's stiffening parameter
$E_1, E_2, E_3$	= Young's moduli (Pa)

$S(t)$	= nominal tensile stress component (Pa)
$G(t)$	= relaxation function
$\tau_k$	= characteristic relaxation times (s)
$g_k$	= relaxation coefficients

## REFERENCES

- [1] Horgan, T. J., and Gilchrist, M. D., 2003, "The creation of three-dimensional finite element models for simulating head impact biomechanics," *Int. J. Crashworthiness.*, 8, pp. 353–366.
- [2] Ho, J., and Kleiven, S., 2009, "Can sulci protect the brain from traumatic injury," *J. Biomech.*, 42, pp. 2074–2080.
- [3] Kleiven, S., and Hardy, W. N., 2002, "Correlation of an FE model of the human head with local brain motion-consequences for injury prediction," *Stapp Car Crash J*, 46, pp. 123–144.
- [4] Kleiven, S., 2007, "Predictors for traumatic brain injuries evaluated through accident reconstructions," *Stapp Car Crash J*, 51, pp. 81–114.
- [5] Takhounts, E. G., Eppinger, R. H., Campbell, J. Q., Tannous, R. E., Power, E. D., and Shook, L. S., 2003, "On the development of the SIMON finite element head model," *Stapp Car Crash J.*, 47, pp. 107–133.
- [6] Zhang, L., Yang, K. H., Dwarampudi, R., Omori, K., Li, T., Chang, K., Hardy, W. N., Khalil, T. B., and King, A. I., 2001, "Recent advances in brain injury research: a new human head model development and validation," *Stapp Car Crash J.*, 45, pp. 369 – 393. .
- [7] Nicolle, S., Lounis, M., and Willinger, R., 2004, "Shear properties of brain tissue over a frequency range relevant for automotive impact situations: New experimental results," *Stapp Car Crash J.*, 48, pp. 239 – 258.
- [8] Margulies, S. S., Thibault, L. E., and Gennarelli, T. A., 1990, "Physical model simulations of brain injury in the primate," *J. Biomech.* , 23, pp. 823-836.
- [9] Meaney, D. F., and Thibault, L. E., 1990, "Physical model studies of cortical brain deformation in response to high strain rate inertial loading," *International Conference on the Biomechanics of Impacts. IRCOBI.*Lyon, France.
- [10] Morrison III, B., Meaney, D. F., Margulies, S. S., and McIntosh, T. K., 2000, "Dynamic mechanical stretch of organotypic brain slice cultures induces differential genomic expression: relationship to mechanical parameters," *J. Biomech. Eng.*, 122, pp. 224 – 230.
- [11] Morrison III, B., Cater, H. L., Wang, C. C., Thomas, F. C., Hung, C. T., Ateshian, G. A., and Sundstrom, L. E., 2003, "A tissue level tolerance criterion for living brain developed with an In Vitro model of traumatic mechanical loading," *Stapp Car Crash J.* , 47, pp. 93-105.
- [12] Morrison, B., Cater, H. L., Benham, C. D., and Sundstrom, L. E., 2006, "An in vitro model of traumatic brain injury utilizing two-dimensional stretch of organotypic hippocampal slice cultures," *J. Neurosci. Methods.*, 150, pp. 192–201.
- [13] Brands, D. W. A., Peters, G. W. M., and Bovendeerd, P. H. M., 2004, "Design and numerical implementation of a 3-D non-linear viscoelastic constitutive model for brain tissue during impact," *J. Biomech*, 37, pp. 127–134.
- [14] Arbogast, K. B., Thibault, K. L., Pinheiro, B. S., Winey, K. I., and Margulies, S. S., 1997, "A high-frequency shear device for testing soft biological tissues," *J. Biomech*, 30, pp. 757–759.
- [15] Bilston, L. E., Liu, Z., and Phan-Tiem, N., 2001, "Large strain behavior of brain tissue in shear: some experimental data and differential constitutive model," *Biorheology.*, 38, pp. 335–345.
- [16] Darvish, K. K., and Crandall, J. R., 2001, "Nonlinear viscoelastic effects in oscillatory shear deformation of brain tissue," *Med. Eng. Phys.*, 23, pp. 633–645.
- [17] Fallenstein, G. T., Hulce, V. D., and Melvin, J. W., 1969, "Dynamic mechanical properties of human brain tissue," *J. Biomech*, 2, pp. 217-226.
- [18] Hrapko, M., van Dommelen, J. A. W., Peters, G. W. M., and Wismans, J. S. H. M., 2006, "The mechanical behaviour of brain tissue: large strain response and constitutive modelling," *Biorheology*, 43(5), pp. 623–636.
- [19] Nicolle, S., Lounis, M., Willinger, R., and Palierne, J. F., 2005, "Shear linear behavior of brain tissue over a large frequency range," *Biorheology.*, 42(3), pp. 209–223.
- [20] Prange, M. T., and Margulies, S. S., 2002, "Regional, directional, and age-dependent properties of the brain undergoing large deformation," *J. Biomech. Eng.*, 124(2), pp. 244–252.
- [21] Shuck, L. Z., and Advani, S. H., 1972, "Rheological response of human brain tissue in shear," *ASME, J. Basic. Eng.* , 94, pp. 905-911.

- [22] Thibault, K. L., and Margulies, S. S., 1998, "Age-dependent material properties of the porcine cerebrum: Effect on pediatric inertial head injury criteria," *J. Biomech.*, 31, pp. 1119-1126.
- [23] Cheng, S., and Bilston, L. E., 2007, "Unconfined compression of white matter," *J. Biomech.*, 40, pp. 117-124.
- [24] Estes, M. S., and McElhaney, J. H., 1970, "Response of brain tissue of compressive loading," *ASME*, pp. Paper No. 70-BHF-13.
- [25] Miller, K., and Chinzei, K., 1997, "Constitutive modelling of brain tissue: experiment and theory," *J. Biomech.*, 30(11-12), pp. 1115 -1121.
- [26] Pervin, F., and Chen, W. W., 2009, "Dynamic mechanical response of bovine grey matter and white matter brain tissues under compression," *J. Biomech.*, 42, pp. 731-735.
- [27] Rashid, B., Destrade, M., and Gilchrist, M. D., 2012, "Mechanical characterization of brain tissue in compression at dynamic strain rates," *J. Mech. Behavior. Biomed. Mat.*, 10, pp. 23-38.
- [28] Tamura, A., Hayashi, S., Watanabe, I., Nagayama, K., and Matsumoto, T., 2007, "Mechanical characterization of brain tissue in high-rate compression," *J. Biomech. Sci. Eng.*, 2(3), pp. 115 - 126.
- [29] Miller, K., and Chinzei, K., 2002, "Mechanical properties of brain tissue in tension," *J. Biomech.*, 35, pp. 483-490.
- [30] Tamura, A., Hayashi, S., Nagayama, K., and Matsumoto, T., 2008, "Mechanical characterization of brain tissue in high-rate extension," *J. Biomech. Sci. Eng.*, 3(2), pp. 263 - 274.
- [31] Velardi, F., Fraternali, F., and Angelillo, M., 2006, "Anisotropic constitutive equations and experimental tensile behavior of brain tissue," *Biomech. Model. Mechanobiol.*, 5(1), pp. 53-61.
- [32] Bain, A. C., and Meaney, D. F., 2000, "Tissue-level thresholds for axonal damage in an experimental model of central nervous system white matter injury," *J. Biomech. Eng.*, 122, pp. 615 - 622.
- [33] Bayly, P. V., Black, E. E., and Pedersen, R. C., 2006, "*In vivo* imaging of rapid deformation and strain in an animal model of traumatic brain injury," *J. Biomech.*, 39, pp. 1086 - 1095.
- [34] Pfister, B. J., Weihs, T. P., Betenbaugh, M., and Bao, G., 2003, "An in vitro uniaxial stretch model for axonal injury," *Ann. Biomed. Eng.*, 31, pp. 589-598.
- [35] Rashid, B., Destrade, M., and Gilchrist, M. D., 2012, "A high rate tension device for characterizing brain tissue," *J. Sports Eng. Tech. Part P*, In press, DOI: 10.1177/1754337112436900.
- [36] Ogden, R. W., 1997, *Non-linear elastic deformations*, Dover, New York.
- [37] Fung, Y. C., 1967, "Elasticity of soft tissues in simple elongation," *Am J Physiol* 213, pp. 1532-1544
- [38] Fung, Y. C., Fronek, K., and Patitucci, P., 1979, "Pseudoelasticity of arteries and the choice of its mathematical expression," *Am J Physiol*, 237, pp. H620-H631
- [39] Gent, A., 1996, "A new constitutive relation for rubber," *Rubber. Chem. Technol.*, 69, pp. 59-61.
- [40] Fung, Y. C., 1993, *Biomechanics: mechanical properties of living tissues*, Springer-Verlag, New York.
- [41] Finan, J. D., Elkin, B. S., Pearson, E. M., Kalbian, I. L., and Morrison III, B., 2012, "Viscoelastic properties of the rat brain in the sagittal plane: Effects of anatomical structure and age," *Ann. Biomed. Eng.*, 40(1), pp. 70-78.
- [42] Elkin, B. S., Ilankovan, A. I., and Morrison III, B., 2011, "Dynamic, regional mechanical properties of the porcine brain: Indentation in the coronal plane," *J. Biomech. Eng.*, 133, p. 071009.
- [43] Rashid, B., Destrade, M., and Gilchrist, M. D., 2012, "Inhomogeneous deformation of brain tissue during tension tests," *Comp. Mat. Sci.*, in press, DOI:10.1016/j.commatsci.2012.05.030.